Applied Catalysis B: Environmental 96 (2010) 557–564

Contents lists available at ScienceDirect

Applied Catalysis B: Environmental

journal homepage: www.elsevier.com/locate/apcatb

Pivotal role of fluorine in enhanced photocatalytic activity of anatase TiO_2 nanosheets with dominant (0 0 1) facets for the photocatalytic degradation of acetone in air

Quanjun Xiang[a], Kangle Lv[a,b], Jiaguo Yu[a,*]

[a] State Key Laboratory of Advanced Technology for Material Synthesis and Processing, Wuhan University of Technology, Luoshi Road 122#, Wuhan 430070, PR China
[b] Key Laboratory of Catalysis and Materials Science of the State Ethnic Affairs Commission & Ministry of Education, South-Central University for Nationalities, Wuhan 430074, PR China

ARTICLE INFO

Article history:
Received 9 December 2009
Received in revised form 10 March 2010
Accepted 11 March 2010
Available online 17 March 2010

Keywords:
TiO_2 nanosheets
{0 0 1} facets
Hydrothermal route
Surface fluorination
Photocatalytic activity

ABSTRACT

Surface-fluorinated anatase TiO_2 nanosheets with dominant {0 0 1} facets were fabricated by a simple hydrothermal route in a $Ti(OC_4H_9)_4$-HF-H_2O mixed solution. The atomic ratios of fluorine to titanium (R_F) exhibit an obvious influence on the structures and photocatalytic activity of TiO_2 samples. In the presence of HF, TiO_2 nanosheets can be easily obtained. With increasing R_F, the relative anatase crystallinity, average crystallite size, pore size and percentage of exposed {0 0 1} facets increase, contrarily, BET specific surface areas decrease. All fluorinated TiO_2 nanosheets exhibit much higher photocatalytic activity than Degussa P-25 TiO_2 (P25) and pure TiO_2 nanoparticles prepared in pure water due to the synergistic effect of surface fluorination and exposed {0 0 1} facets on the photoactivity of TiO_2. Especially, at $R_F = 1$, the fluorinated TiO_2 nanosheet exhibits the highest photocatalytic activity, and its photoactivity exceeds that of P25 by a factor of more than nine times.

1. Introduction

A great deal of efforts have been devoted in recent years to developing oxide semiconductor photocatalysts with high activities for environmental protection procedures such as air purification, water disinfection, hazardous waste remediation, and water purification [1–8]. Among various oxide semiconductor photocatalysts, titania has been proven to be the most suitable for widespread environmental applications due to its biological and chemical inertness, strong oxidizing power, cost effectiveness, long-term stability against photocorrosion and chemical corrosion. However, the photocatalytic activity of titania must be further enhanced from the point of view of practical use and commerce [9–12]. To achieve this purpose, various strategies such as doping, metal deposition, surface sensitization and coupling of composite semiconductors, have been developed over recent decades [4,11,12]. In particular, it is demonstrated that photocatalytic activity of titania is strongly dependent on its phase structures, surface hydroxyl content, crystallinity, the surface areas, crystalline size and shape (or facets exposed on the surface) [13,14].

Recently, the role of fluorine has attracted increasing attention of researchers in the photocatalytic field because of its capability to improve the photocatalytic activity and to control the synthesis of TiO_2 [15–25]. Lu and co-workers reported the synthesis of anatase TiO_2 microcrystals with highly energetic {0 0 1} facets through the use of hydrofluoric acid as a shape controlling agent [24]. Han and co-workers used a similar strategy to synthesize anatase TiO_2 nanosheets with 89% exposed {0 0 1} facets using hydrofluoric acid solution as the solvent [25]. Since the (0 0 1) surface of anatase TiO_2 nanosheets is much more reactive than the thermodynamically stable (1 0 1) surface, the obtained nanosheets will offer new chance to design highly active photocatalytic materials and devices [26–28].

It is well-known that heterogeneous photocatalytic reactions primarily take place on the surface of TiO_2 and its surface properties are critical for the enhancement of photocatalytic efficiencies [29,30]. Surface fluorination of TiO_2 has been intensively studied as a new method of surface modification [28–37]. It has been reported that the OH radical-mediated photocatalytic degradation reactions are greatly accelerated on surface fluorination TiO_2 (F-TiO_2). For example, Pelizzetti and co-workers reported that surface fluorination of TiO_2 could improve the photocatalytic oxidation rate of phenol in aqueous solution. Mrowetz and Selli also reported direct experimental evidence on more hydroxyl radicals generated on fluorinated titanium dioxide obtained by spin-trapping EPR measurements and the faster photoinduced bleaching of the azo dye Acid Red 1 (AR1) in the presence of F-TiO_2 [38,39]. Furthermore, Choi and his colleagues have recently found that F-TiO_2 could

* Corresponding author. Tel.: +86 27 87871029; fax: +86 27 87879468.
E-mail address: jiaguoyu@yahoo.com (J. Yu).

0926-3373/$ – see front matter © 2010 Elsevier B.V. All rights reserved.
doi:10.1016/j.apcatb.2010.03.020

enhance the remote photocatalytic oxidation at the air/catalyst interface by facilitating the desorption of OH radicals under UV irradiation [29]. From these researches, it can be inferred that the introduction of fluorine, irrespective of fluorination approaches, really enhances the photocatalytic activity of TiO_2. However, to the best of our knowledge, the effects of HF concentration on photocatalytic activity of anatase TiO_2 nanosheets with dominant {0 0 1} facets for the photocatalytic decomposition of acetone in air have been considered less often.

In this study, surface-fluorinated anatase TiO_2 nanosheets are synthesized in a large scale via a simple hydrothermal route using tetrabutyl titanate ($Ti(OC_4H_9)_4$) as a titanium source and HF solution as the solvent. We also carefully investigate the influences of HF content on the microstructures and photocatalytic activity of TiO_2 samples. This work is obviously different from the recently reported work by Han et al. because their results indicate the photocatalytic degradation efficiency of methyl orange (MO) in aqueous solution is remarkably enhanced by removal of surface fluorine ions on TiO_2 [25]. Contrarily, in our study, surface fluorination can significantly enhance the photocatalytic activity of TiO_2 nanosheets because the strong electron-withdrawing ability of the surface ≡Ti–F groups reduces the recombination of photo-generated electrons and holes, and enhances the formation of free OH radicals.

2. Experimental

2.1. Sample preparation

Anatase TiO_2 nanosheets were prepared using a hydrothermal method similar to that described by Han et al. [25]. In a typical preparation procedure, 25 mL of $Ti(OC_4H_9)_4$ and 3 mL of hydrofluoric acid solution (with a concentration 40 wt.%) were mixed in a dried Teflon-lined autoclave with a capacity of 100 mL at room temperature, and then kept at 180 °C for 24 h. The nominal atomic ratio of fluorine to titanium (R_F) was 1. After hydrothermal reaction, the white precipitates were collected, washed with ethanol and distilled water for three times, and then dried in an oven at 80 °C for 6 h. To investigate the effects of HF concentration on morphology and photocatalytic activity of anatase TiO_2 nanosheets, R_F varied from 0 to 2.67 (0, 0.67, 1, 1.33 and 2.67) by varying the volume of hydrofluoric acid. At $R_F = 0$, 3 mL of hydrofluoric acid solution was replaced by 3 mL of distilled water.

2.2. Characterization

Morphological observations were performed on an S-4800 field emission scanning electron microscope (SEM, Hitachi, Japan) and linked with an Oxford Instruments X-ray analysis system. Transmission electron microscopy (TEM) and high-resolution transmission electron microscopy (HRTEM) analyses were conducted with a JEM-2100F electron microscope (JEOL, Japan), using a 200 kV accelerating voltage. The X-ray diffraction (XRD) measurements, which were used to characterize the crystalline phase, phase composition and crystallite size of the TiO_2 powders, were carried out by an X-ray diffractometer (type HZG41B-PC) using Cu Kα radiation at a scan rate of $0.05^\circ\ 2\theta\ s^{-1}$. The accelerating voltage and applied current were 40 kV and 80 mA, respectively. The Brunauer–Emmett–Teller (BET) specific surface area (S_{BET}) of the powders was analyzed by nitrogen adsorption in a Micromeritics ASAP 2020 nitrogen adsorption apparatus (USA). All the as-prepared samples were degassed at 180 °C prior to nitrogen adsorption measurements. The BET surface area was determined by a multipoint BET method using the adsorption data in the relative pressure (P/P_0) range of 0.05–0.3. A desorption isotherm was used to determine the pore size distribution via the Barret–Joyner–Halender (BJH) method, assuming a cylindrical pore modal [14,40]. The nitrogen adsorption volume at the relative pressure (P/P_0) of 0.994 was used to determine the pore volume and average pore size. The X-ray photoelectron spectroscopy (XPS) measurement was made in an ultrahigh vacuum VG ESCALAB 210 electron spectrometer equipped with a multichannel detector. The spectra were excited using Mg Kα (1253.6 eV) radiation (operated at 200 W) of a twin anode in the constant analyser energy mode with a pass energy of 30 eV. All the binding energies were referenced to the C 1s peak at 284.8 eV of the surface adventitious carbon. Photoluminescence (PL) spectra were measured at room temperature on a Fluorescence Spectrophotometer (F-7000, Hitachi, Japan). The excitation wavelength was 300 nm, the scanning speed was 1200 nm/min, and the PMT voltage was 700 V. The width of excitation slit and emission slit were both 5.0 nm.

2.3. Evaluation of photocatalytic activity

It is well known that volatile organic compounds (VOCs) are triggering serious environmental problems such as stratospheric ozone depletion and tropospheric ozone increase, depending on their chemical structures. Furthermore, some of these volatile organic compounds in the indoor air are also arousing health disorders, such as leukemia, nausea, headache and fatigue. Degradation of acetone in air is particularly important because it is the principle indoor air pollutant. Therefore, we chose acetone as a model contaminate chemical. Photocatalytic oxidation of acetone is based on the following reaction [41–43]:

$$CH_3COCH_3 + 4O_2 \rightarrow 3CO_2 + 3H_2O \quad (1)$$

The photocatalytic activity experiments on the as-prepared TiO_2 samples and P25 were performed according to the reported procedures [13,16]. The weight of the photocatalyst used for each experiment was kept at about 0.2 g. The analysis of acetone, carbon dioxide, and water vapor concentration was on-line conducted with a Photoacoustic IR Multigas Monitor (INNOVA Air Tech Instruments Model 1412). The initial concentration of acetone after the adsorption equilibrium was about 300 ± 20 ppm, which remained constant for about 5 min until a 15 W, 365 nm UV lamp (4 cm above the dishes) (Cole-Parmer Instrument Co., USA) in the reactor was switched on. Integrated UV intensity in the wavelength range of 310–400 nm striking the samples measured with a UV radiometer (UV-A, China) was 2.9 mW/cm^2, while the peak wavelength of UV light was 365 nm. During the photocatalytic reaction, a near 3:1 ratio of carbon dioxide products to acetone destroyed was observed, and the acetone concentration decreased steadily with UV illumination time. Our previous and present experiments indicated that all acetone was converted to CO_2 and H_2O and no other intermediate products were observed. Each set of experiment was followed for 60 min. The photocatalytic activity of the powders can be quantitatively evaluated by comparing the apparent reaction rate constants. The photocatalytic degradation of acetone is a pseudo-first-order reaction and its kinetics may be expressed as follows: $\ln(C_0/C) = kt$, where k is the apparent reaction rate constant, and C_0 and C are the initial concentration and the reaction concentration of acetone, respectively. To further determine the effect of surface fluorination on the photoactivity of TiO_2 nanosheets, the fluorinated TiO_2 nanosheets are cleaned by high-temperature calcinations at 600 °C or 0.1 M NaOH solution rinse [24,25]. The photocatalytic activity of the cleaned TiO_2 nanosheets is also measured at the same experimental conditions.

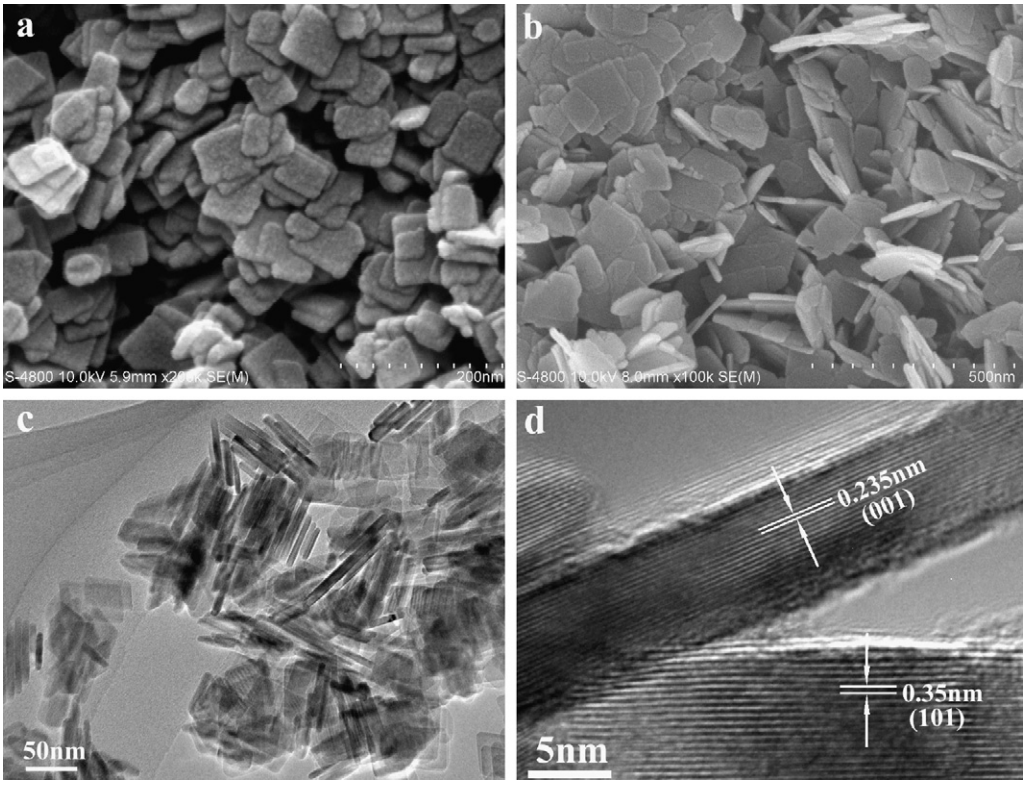

Fig. 1. SEM (a, b), TEM (c) and HRTEM (d) images of the fluorinated TiO_2 samples prepared with varying R_F: $R_F = 1$ (a, c, d) and $R_F = 2.67$ (b).

3. Results and discussion

3.1. Morphology and phase structures

TiO_2 nanosheets with dominant {0 0 1} facets are easily fabricated by a simple hydrothermal method (see Section 2). Fig. 1a shows a typical SEM image for the TiO_2 sample prepared at $R_F = 1$. A large amount of nanosheets with side length of ca. 50 nm, and thickness of ca. 10 nm can be easily observed. Increasing R_F to 2.67, it is interesting to note that the side length of nanosheets increases to ca. 100 nm, meanwhile, the sheet thickness slightly increases to ca. 15 nm (see Fig. 1b). This also implies that with increasing R_F, the percentage of the top and bottom areas to the total surface area of nanosheets increases. TEM images further show that the product prepared at $R_F = 1$ consists of well-defined sheet-shaped structures having a rectangular outline, with an average side size of about 50 nm (Fig. 1c), similar to the SEM observations. The high-resolution TEM image (Fig. 1d) directly shows that the lattice spacing parallel to the top and bottom facets is ca. 0.235 nm, corresponding to the (0 0 1) planes of anatase TiO_2, which indicates the top and bottom facets of the nanosheets are the (0 0 1) and (0 0 −1) planes, respectively. Another set of the lattice fringes with spacing of 0.35 nm, corresponding to the (1 0 1) planes of anatase, can be also clearly revealed from the sheets lying on the TEM grid. On the basis of the SEM, TEM and HRTEM results, we can calculate the percentage of exposed {0 0 1} facets on the TiO_2 nanosheets and the calculated results are shown in Table 1. It can be seen that with increasing R_F from 0.67 to 2.67, the average percentage of exposed {0 0 1} facets on the TiO_2 nanosheets increase from 61 to 78%. However, in pure water ($R_F = 0$), the product consists of a large amount of aggregated nanoparticles (not shown here). According to the theory estimation and experimental results, the percentage of exposed {0 0 1} facets for the TiO_2 nanoparticles is less than 10% (ca. 6%) [25]. This indicates that the fluorine ions play a key role in the formation of TiO_2 nanosheets with high percentage of exposed {0 0 1} facets. XRD patterns of the TiO_2 samples prepared with varying R_F further confirm the formation of anatase [JCPDS No. 21-1272, space group: $I4_1/amd$ (141)] in each case (see Fig. 2 and Table 1). All the prepared TiO_2 samples display a good crystallinity. Further observation shows that with increasing R_F, XRD peak intensities of anatase steadily increase and the width of peaks becomes narrower, indicating the formation of greater TiO_2 crystallites and an

Table 1
Effects of R_F on the physicochemical properties of TiO_2 samples.

R_F	Phase[a]	Crystalline size (nm)	S_{BET} (m^2/g)	Average pore size	Pore volume (cm^3/g)	Porosity (%)	Relative crystal[b]	Percentage of {0 0 1}
0	A	8.9	156	7.4	0.33	55.0	1	<10 ± 1
0.67	A	12.5	128	8.8	0.35	56.5	1.46	61 ± 6
1	A	13.6	114	16.0	0.52	65.8	1.68	71 ± 7
1.33	A	15.1	108	19.0	0.53	66.3	1.73	74 ± 7
2.67	A	17.9	97	20.0	0.56	67.5	1.95	78 ± 9
P25	A, R	30 (A)	55.1	3.9	0.06	18.2	–	–

Surface-fluorinated anatase TiO_2 nanosheets with dominant {0 0 1} facets are fabricated by a simple hydrothermal route and their photocatalytic activity is more than 9 times higher than that of P25.

[a] A and R denote anatase and rutile, respectively.

[b] Relative anatase crystallinity: the relative intensity of the diffraction peak from the anatase (1 0 1) plane (reference = the sample prepared at $R_F = 0$).

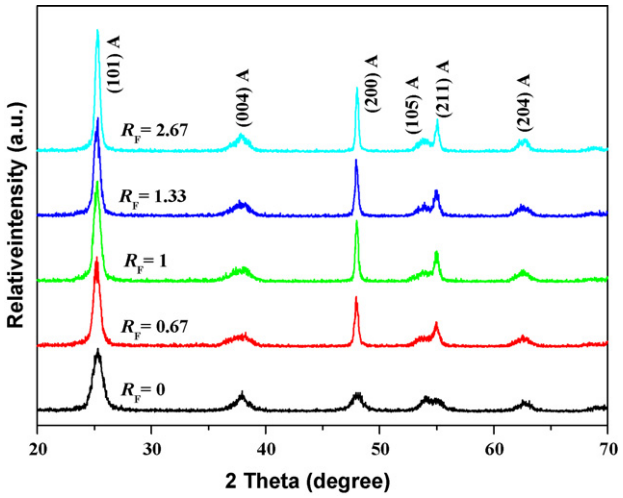

Fig. 2. XRD patterns of the TiO_2 samples prepared with varying R_F.

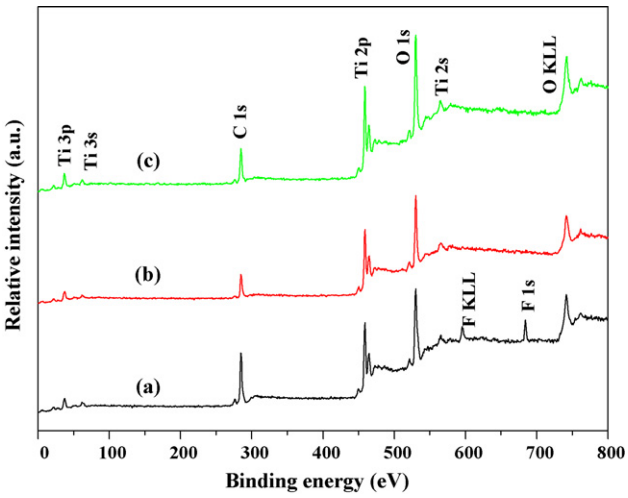

Fig. 4. XPS survey spectra of the R_F = 1 TiO_2 samples un-treated (a) and treated (b and c) by the different methods: (b) washed by 0.1 M NaOH solution and (c) calcined at 600 °C for 2 h.

enhancement of crystallization. This is in good agreement with our previous report that fluoride enhances the crystallization of anatase phase and promotes the growth of crystallites [13,28].

3.2. BET surface areas and pore size distributions

Nitrogen adsorption–desorption isotherms were measured to determine the specific surface areas and pore size distribution of the TiO_2 samples prepared with varying R_F values (see Fig. 3). The isotherms corresponding to the sample prepared at R_F = 0 are of type IV (Brunauer–Deming–Deming–Teller (BDDT) classification), as indicated by a hysteresis loop at high relative pressures associated with capillary condensation of gases within mesopores (2–50 nm) [14,40,44]. The hysteresis loop is of type H2, which is consistent with pores with narrow necks and wider bodies (ink-bottle pores). The pore size distribution (inset) calculated from the desorption branch of the nitrogen isotherm by the BJH (Barrett–Joyner–Halenda) method shows a narrow range of 6.0–12.0 nm with a maximum pore diameter of about 9.0 nm [14,40,44]. The presence of fluoride in the synthesis mixture exerts a significant influence on the pore structure and BET surface areas of the obtained products (Table 1). With increasing R_F, the average pore size and pore volume increase and the BET surface areas decrease due to growth of TiO_2 crystallites. Furthermore, in the presence of fluoride, the shapes of the hysteresis loops change from type H2 to H3, indicating the presence of slit-like pores. The isotherms show high absorption at high relative pressure (P/P_0) range (approaching 1.0), indicating the formation of large mesopores and macropores. In fact, the single-crystal nanosheets do not contain mesopores and macropores. Therefore, the existing nanopores (or pore volume) are from the aggregation of nanosheets. Such organized porous structures might be extremely useful in photocatalysis as they would provide efficient transport pathways to reactant and product molecules. Table 1 also shows quantitative details on BET surface area, pore volume, porosity and average pore size of the TiO_2 samples prepared at different R_F values. In general, the samples show an increase in average pore size, pore volume and porosity, but a slightly decrease in the BET surface area with increasing R_F. This is ascribed to the fact that the greater the amount of F^- ions in the reaction solution, the stronger the promoting effect on growth of TiO_2 anatase crystallites, and the larger the size of TiO_2 nanosheets.

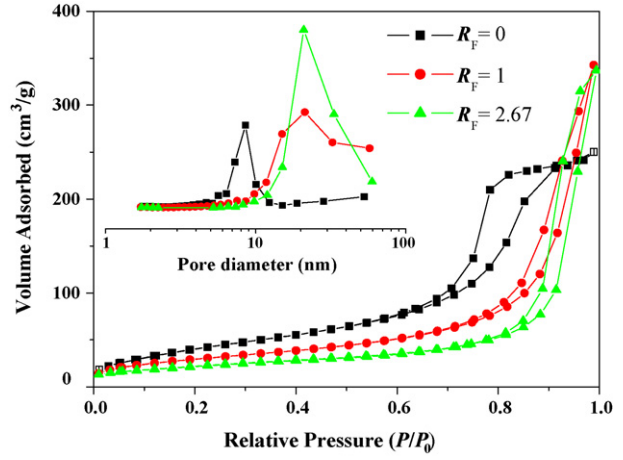

Fig. 3. Nitrogen adsorption–desorption isotherms and their corresponding pore size distribution curves (inset) of the TiO_2 samples prepared with varying R_F.

3.3. XPS analysis

Fig. 4a shows XPS survey spectrum of a typical fluorinated TiO_2 sample prepared at R_F = 1. Sharp photoelectron peaks appear at binding energies of 458 (Ti 2p), 531 (O 1s), 684 (F 1s) and 285 eV (C 1s). The carbon peak is attributed to the residual carbon from the sample and adventitious hydrocarbon from XPS instrument itself. Fig. 5a shows the high-resolution XPS spectrum of F 1s region. The measured binding energy is 684.5 eV, which is a typical value for fluorinated TiO_2 systems such as ≡Ti–F species on the TiO_2 crystal surface. No signal for F^- in the lattice of TiO_2 (BE = 688.5 eV) is found [16,28,45]. Furthermore, the binding energies of Ti $2p_{3/2}$ and Ti $2p_{1/2}$ are equal to 458.9 and 464.4 eV, respectively (see Fig. 5b), which are identical to that of Ti^{4+} of bulk TiO_2. Therefore, It can be easily concluded from the above XPS results that the F-doping of anatase TiO_2 crystal lattice (the atomic incorporation of F atoms and/or their substitution for O atoms) can be completely ruled out and F element only exists in surface fluoride (≡Ti–F) [6,24,45]. This is not difficult to understand because, on the one hand, the hydrothermal environment can accelerate crystallization of TiO_2 due to the in situ dissolution–recrystallization process, resulting in the reduction of the number of defects and impurity in TiO_2 crystals, on the other hand, surface fluorination can be easily carried out by a simple ligand exchange reaction between surface hydroxyl groups on TiO_2 and fluoride anions (F^-) due to the high

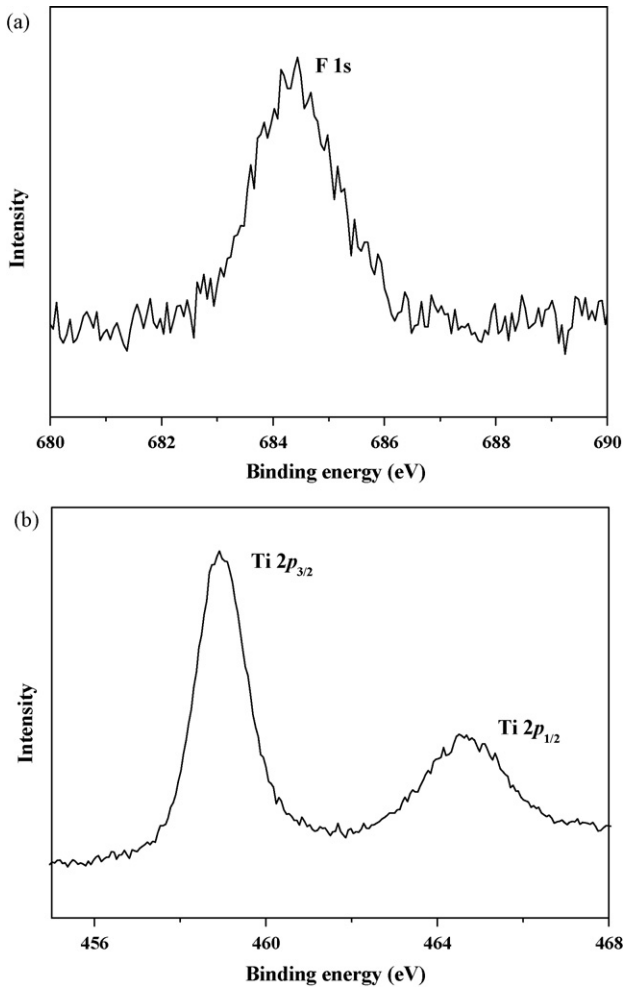

Fig. 5. High-resolution XPS spectra of F 1s (a) and Ti 2p (b) of the fluorinated TiO_2 sample prepared at $R_F = 1$.

F–Ti bonding energy. Therefore, it is not surprising that the surface fluorination modification of TiO_2 readily takes place under a strongly acidic hydrothermal environment. The actual amount of F in the F-TiO_2 nanosheets prepared at $R_F = 1$ is 5.69%, which is lower than that of the precursor solution. This is easy to understand because F^- is only adsorbed on the surface of F-TiO_2 sample. With increasing R_F (from 0.67, 1, 1.33 to 2.67), the actual amount of corresponding fluorine slightly increases (from 4.87, 5.69, 6.42 to 6.86) due to the saturation adsorption of F^- on the TiO_2 surface. It is well known that the fluorination on the surface of TiO_2 can accelerate the photocatalytic degradation of a wide range of organic pollutants since the •OH radicals generated on the surface of F-TiO_2 are more mobile than those generated on pure TiO_2 under UV irradiation (reactions (2) and (3)) [46]:

$$\equiv \text{Ti–OH} + h_{vb}{}^{+} \leftrightarrow \equiv \text{Ti–OH}^{\bullet +} \quad (2)$$

$$\equiv \text{Ti–F} + \text{H}_2\text{O}(\text{or OH}^-) + h_{vb}{}^{+} \rightarrow \equiv \text{Ti–F} + {}^{\bullet}\text{OH}_{free} + \text{H}^+ \quad (3)$$

Also, the redox potential of free OH radicals in solution (ca. 2.3 V vs NHE at pH 7) is larger than that of surface-adsorbed OH radicals on TiO_2 (about 1.5–1.7 V vs NHE at pH 7) [28].

3.4. PL spectra

The PL emission spectra can be used to disclose the efficiency of charge carrier trapping, immigration, transfer and separation, and to understand the fate of photo-generated electrons and holes in semiconductor since PL emission results from the recombination of free carriers [16,47]. Fig. 6 shows comparison of PL spectra of pure and fluorinated TiO_2 samples prepared with varying R_F values in the wavelength range of 350–550 nm. All the emission spectra shapes are similar and three main emission peaks appear at about 398, 451 and 468 nm, which are equivalent to 3.12, 2.75 and 2.65 eV, respectively. A strong peak at about 398 nm is attributed to the emission of band gap transition with the energy of light approximately equal to the bandgap energy of anatase (387.5 nm). In addition, there are four small peaks observed in the wavelength range from 440 to 500 nm. These PL signals are due to excitonic PL, which mainly result from surface oxygen vacancies and defects of the TiO_2 samples. The PL peaks at 451 and 468 nm are attributed to band edge free excitons, and other two peaks at 483 and 493 nm are attributed to bound excitons [16,47]. Fig. 6 also shows a decrease in emission intensity between the sample prepared at $R_F = 0$ and $R_F = 1$. This indicates that an appropriate amount of F^- can significantly reduce the radiative recombination rate of photo-generated electrons and holes in TiO_2. The sample prepared with excessive HF (at $R_F = 2.67$), however, exhibits a significant increase in the emission intensity and its intensity is still smaller than that of the pure TiO_2 samples prepared at $R_F = 0$. This is due to the introduction of new defect sites (or recombination centers) that enhances the recombination of photo-generated electrons and holes. Our PL measurement results also imply that the lower the intensity of PL spectra of the samples is, the higher the photocatalytic activity.

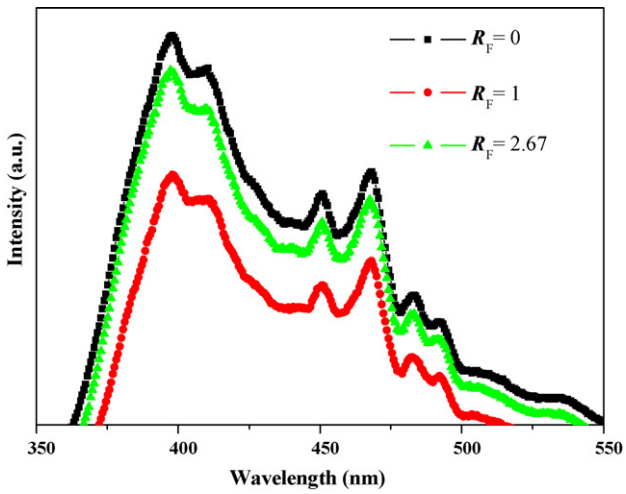

Fig. 6. PL spectra of the TiO_2 samples prepared with varying R_F.

3.5. Photocatalytic activity

The photoctalytic activity of the as-prepared TiO_2 samples was evaluated by gaseous photocatalytic oxidation decomposition of acetone. Fig. 7a and b displays a comparison of photocatalytic activity (or apparent reaction rate constants) of the TiO_2 samples prepared with varying R_F and P25 and the dependence of corresponding produced CO_2 concentration (ppm) on R_F, respectively. It can be seen that R_F exhibits a significant influence on the photocatalytic activity of the TiO_2 samples. At $R_F = 0$, the pure TiO_2 sample prepared in pure water shows a good photocatalytic activity and its k reaches 3.65×10^{-3}. This is due to the pure TiO_2 sample with anatase phase structure, high specific surface areas and small crystallite size (see Table 1). It should be noted that the activity of all fluorinated TiO_2 powders is markedly higher than that of the pure TiO_2 and P25. With increasing R_F from 0 to 1, the photocatalytic activity of fluorinated TiO_2 samples significantly increased. At $R_F = 1$, the k reaches the highest value and its value

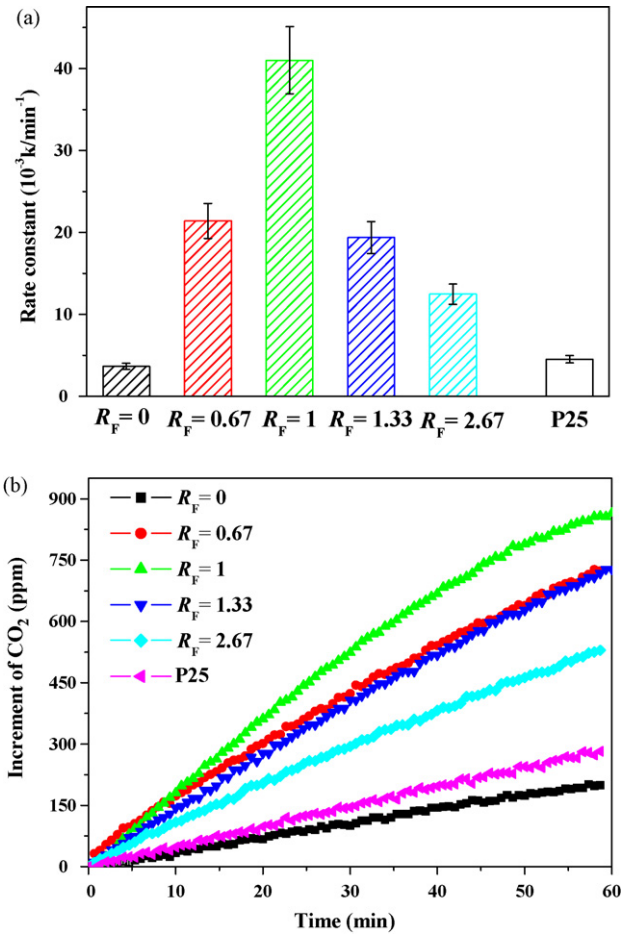

Fig. 7. (a) Comparison of photocatalytic activity of P25 and the TiO_2 samples prepared with varying R_F for photocatalytic decomposition of acetone. (b) The dependence of corresponding produced CO_2 concentration (ppm) on R_F.

was 41.1×10^{-3}. It is well known that P25 has excellent photocatalytic activity [28,48,49]. The k value of P25 was determined to be 4.5×10^{-3} for 0.2 g sample at the same experimental conditions. Surprisingly, the photocatalytic activity of the $R_F = 1$ sample much exceeds that of P25 by a factor of 9.1. To the best of our knowledge, this is our first time to find and report surface-fluorinated TiO_2 nanosheets with exposed {0 0 1} facets exhibiting excellent photocatalytic activity for oxidation decomposition of acetone in air under UV light illumination. With further increasing R_F values, the k decreases rapidly. This indicates that the photocatalytic activity of F-TiO_2 nanosheets is strongly dependent on the HF concentration in the solution since the adsorbed F^- ions can serve not only as a mediator of interfacial charge transfer but also as a recombination center [28]. Of course, the higher the HF concentration is, the more the adsorbed F^- on TiO_2 nanosheets. In our case an optimal HF concentration is $R_F = 1$. Above this concentration, the adsorbed F^- ions steadily become recombination centers of photo-generated electrons and holes, resulting in the reduction of the activity.

Why is the photocatalytic activity of all F-TiO_2 nanosheets much higher than that of the pure TiO_2 powders and P25? This can be mainly ascribed to the synergetic effects of two factors including the exposure of highly reactive {0 0 1} facets of nanosheets (see Fig. 1) and their surface fluorination (Figs. 4 and 5a). First, theoretical and experimental studies have indicated that the (0 0 1) surface of anatase TiO_2 is much more reactive than the thermodynamically more stable (1 0 1) surface and the {0 0 1} facets are the dominant source of active sites for photocatalytic oxidation reactions [50,51]. However, most synthetic anatase nano-crystals

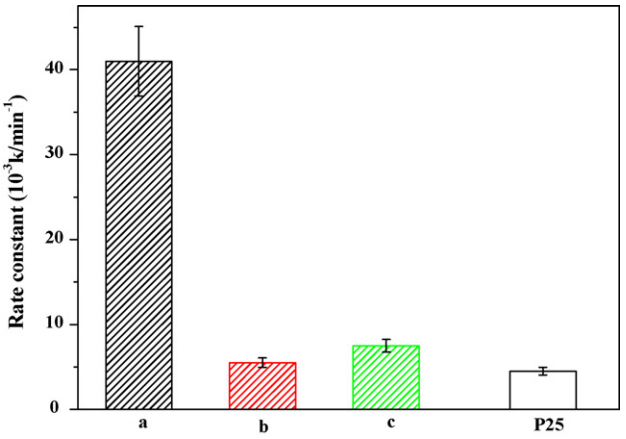

Fig. 8. Comparison of the apparent rate constants of P25 and the $R_F = 1$ TiO_2 samples treated by the different methods: (a) washed by H_2O, (b) washed by 0.1 M NaOH solution and (c) calcined at 600 °C for 2 h.

are dominated by the less-reactive {1 0 1} facets. Therefore, it is not difficult to understand that the prepared TiO_2 nanosheets with exposed {0 0 1} facets show higher photocatalytic activity than TiO_2 nanoparticles [24,50,51]. Second, the surface ≡Ti–F group on the surface of nanosheets can greatly reduce the recombination rate of photo-generated electrons and holes, because it can act as an electron-trapping site to trap the photo-generated electrons by tightly holding trapped electrons due to the strong electronegativity of the fluorine and then transfer them to O_2 adsorbed on the surface of TiO_2 [28]. Therefore, the existence of a suitable amount of F^- ions on the surface of TiO_2 results in the reduction of the recombination rate of electron and hole and enhancement of photocatalytic activity. The previous investigations [28,38,39] have indicated that the formation rate of free OH radicals on F-TiO_2 is much greater than that of surface-bound OH radicals on pure TiO_2. Also, free OH radicals have stronger oxidation ability than surface-adsorbed OH radicals on pure TiO_2 [28]. It should be also noted that the enhancement method for photocatalytic activity in this study is slightly different from our recent report on preparation of mesoporous surface-fluorinated TiO_2 nano-powders of anatase phase [28], because the photocatalytic activity of surface-fluorinated anatase TiO_2 nanosheets with dominant {0 0 1} facets is much higher than that of surface-fluorinated anatase TiO_2 nanoparticles with less exposed {0 0 1} facets. This further indicates that the morphology of TiO_2 particles has a great influence on their photocatalytic activity and TiO_2 nanosheet with exposed {0 0 1} facet is a better photocatalytical candidate material.

To further confirm the synergistic effect of surface fluorination and exposed {0 0 1} facets on the photoactivity of TiO_2, the fluorinated surface of TiO_2 nanosheets was cleaned by high-temperature heat treatment or NaOH diluted solution washing. It has been reported that the adsorbed fluorine ions on the surface of TiO_2 can be easily removed by heat-treatment at 600 °C or alkaline washing in a NaOH solution without altering the crystal structure and morphology [24,25]. In this study, the fluorinated TiO_2 nanosheets were calcined at 600 °C for 2 h, or washed using 0.1 M NaOH solution or distilled water, and then the photocatalytic activity of the treated samples was tested. Fig. 8 presents a comparison of photocatalytic activity of P25 and the $R_F = 1$ TiO_2 nanosheet samples treated by three different methods. It can be seen that water rinse has no obvious influence on the photocatalytic activity of TiO_2 nanosheets. This is not difficult to understand because water rinse has no influence on the morphology and surface chemical composition of TiO_2 nanosheets. However, after the sample was first washed by 0.1 M diluted NaOH solution one time, then washed by distilled water

three times, the photocatalytic activity of the TiO_2 nanosheets drastically decreases. This is due to the fact that F^- on the surface of TiO_2 nanosheets is removed by a simple ligand exchange reaction between OH^- in the NaOH solution and F^- on TiO_2.

$$\equiv Ti–F + OH^- \leftrightarrow \equiv Ti–OH + F^- \quad (4)$$

XPS result (see Fig. 4b) further confirms that the surface F^- is completely removed by NaOH solution washing, also, no Na^+ is found in the treated sample. This implies that fluorine plays a pivotal role in the enhancement of photocatalytic activity of TiO_2 nanosheets. This also further confirms the beneficial effects of surface fluorination on photocatalytic reaction [28,51]. However, this result is different from the previously reported result by Han et al. probably due to different photocatalytic reaction and experimental conditions [25]. We mainly investigate gaseous photocatalytic decomposition of acetone in air. Contrarily, they investigate the photocatalytic decolorization of methyl orange in water. Further investigation shows that when the $R_F = 1$ sample is calcined at 600 °C, the photocatalytic activity of the sample also has a great decrease due to the removal of surface F^- from TiO_2 nanosheets (see XPS result in Fig. 4c) and its activity is still slightly higher than that of the NaOH-cleaning sample probably due to the enhancement of TiO_2 crystallization. Further observation shows that the rate constants of both fluorine-free samples are higher than that of pure TiO_2 and P25 due to the fluorine-free TiO_2 nanosheets with the higher percentage {0 0 1} facets, which are very reactive because of their special electronic and surface structures [50–53]. Our previous investigation also indicates that surface fluorination can enhance the photocatalytic activity of TiO_2 nanoparticles by a factor of ca. 3 times. The above experiments enough prove the synergistic enhancement effect of surface fluorination and exposed {0 0 1} facets on the photoactivity of TiO_2.

Why does the sample prepared at $R_F = 2.67$ with exposure of the highest percentage {0 0 1} facets (78%) not show the highest photocatalytic activity? A possible explanation is that the exposure of the highest percentage of anatase {0 0 1} facets is not suitable for the most highly efficient photocatalytic reaction [54]. Many investigations have indicated that for anatase particles, the oxidation reaction mainly occurs on the {0 0 1} facets and the reduction reaction mainly occurs on the {1 0 1} facets [52,55,56]. This implies that photo-generated holes mainly transfer to {0 0 1} facets, contrarily, photo-generated electrons mainly transfer to {1 0 1} facets. Therefore, it is not difficult to understand that with increasing the percentage of {0 0 1} facets (from nanoparticles to nanosheets) (see Table 1), the photocatalytic activity first rapidly increases (see Fig. 7). However, when the percentage of {0 0 1} facets exposed is higher than 71%, the photocatalytic activity decreases. This is due to the fact that lower percentage of {1 0 1} facet is not beneficial for the transfer and separation of photo-generated electrons and holes and their synergistic effect on photoactivity. Therefore, it is not surprising that the relative percentage of the exposed {0 0 1} and {1 0 1} facets is a very important parameter for the effective separation of photo-generated electrons and holes and has a significant influence on the photocatalytic activity. In our case, the TiO_2 nanosheet sample prepared at $R_F = 1$ possesses an optimal relative percentage (ca. 70%) of anatase {0 0 1} facets, resulting in the best photocatalytic activity observed. So, when R_F is higher than 1, the further increase of the percentage of {0 0 1} facets results in the decrease of photocatalytic activity. Of course, further works are still required to explain the detailed mechanism on the relationship between the percentage of exposed {0 0 1} facets and photocatalytic activity.

The stability of surface-fluorinated anatase TiO_2 nanosheets was further investigated by the recycle experiments of photocatalyst prepared at $R_F = 1$ (not shown here). After five recycles for the photocatalytic oxidation decomposition of acetone in air under UV light illumination, the photocatalytic activity of the sample slightly decreased probably due to adsorption of acetone, CO_2 and H_2O molecules on the surface of TiO_2 nanosheets, resulting in the decrease of active sites. However, the F content does not exhibit any significant loss after five cycles, because the adsorbed fluoride on the surface of TiO_2 does not escape from the surface into the air under UV light illumination. Also, the photocatalytic activity can be easily recovered by heating the samples at 100 °C to remove the adsorbed molecules.

4. Conclusions

Anatase TiO_2 nanosheets with exposed {0 0 1} facets can be prepared by a simple hydrothermal method in the presence of HF. The concentration of HF exhibits a great influence on the morphology, crystallinity, crystallite size and photocatalytic activity of the TiO_2 samples. A higher R_F value results in an increase in relative anatase crystallinity, average crystallite size, pore size and percentage of exposed {0 0 1} facets, contrarily, a decrease in BET specific surface areas. All fluorinated TiO_2 nanosheet samples show higher photocatalytic activity than P25 and pure TiO_2 sample obtained in the absence of HF due to the synergistic effect of surface fluorination and exposed {0 0 1} facets on the photoactivity of TiO_2. At $R_F = 1$, the fluorinated TiO_2 nanosheet sample exhibits the highest photocatalytic activity for photocatalytic oxidation decomposition of acetone in air, and its rate constant k exceeds that of P25 by a factor of more than 9 times, suggesting the existence of an optimal relative percentage (ca. 70%) of exposed anatase {0 0 1} facets. This study will deepen the understanding of the mechanisms of photocatalytic reaction. The prepared surface-fluorinated TiO_2 nanosheets are also of great interest in solar cells, photonic and optoelectronic devices, sensors, catalysis, biomedical engineering and nanotechnology.

Acknowledgements

This work was partially supported by the National Natural Science Foundation of China (50625208, 20773097 and 20877061). This work was also financially supported by the National Basic Research Program of China (2007CB613302 and 2009CB939704) and CHCL09006.

References

[1] A. Fujishima, K. Honda, Nature 238 (1972) 37.
[2] M.R. Hoffmann, S.T. Martin, W. Choi, D.W. Bahnemann, Chem. Rev. 95 (2002) 69.
[3] L.G. Devi, B.N. Murthy, S.G. Kumar, Chemosphere 76 (2009) 1163.
[4] W. Choi, A. Termin, M.R. Hoffmann, J. Phys. Chem. 94 (1994) 13669.
[5] J.G. Yu, H.G. Yu, H.T. Guo, M. Li, S. Mann, Small 4 (2008) 87.
[6] S.W. Liu, J.G. Yu, S. Mann, J. Phys. Chem. C 113 (2009) 10712.
[7] J.G. Yu, Q.J. Xiang, M.H. Zhou, Appl. Catal. B 90 (2009) 595.
[8] A.H. Lu, Y. Li, M. Lv, C.Q. Wang, L. Yang, J. Liu, Y.H. Wang, K.H. Wong, P.K. Wong, Sol. Energy Mater. Sol. C 91 (2007) 1849.
[9] Y.W. Cheng, R.C.Y. Chan, P.K. Wong, Water Res. 41 (2007) 842.
[10] J.H. Park, S. Kim, A.J. Bard, Nano Lett 6 (2006) 24.
[11] M. Ksibi, S. Rossignol, J.M. Tatibouet, C. Trapalis, Mater. Lett. 62 (2008) 4204.
[12] L.G. Devi, N. Kottam, S.G. Kumar, J. Phys. Chem. C 113 (2009) 15593.
[13] J.G. Yu, S.W. Liu, H.G. Yu, J. Catal. 249 (2007) 59.
[14] J.G. Yu, J.C. Yu, M.K.P. Leung, W.K. Ho, B. Cheng, X.J. Zhao, J.C. Zhao, J. Catal. 217 (2003) 69.
[15] H. Park, W. Choi, J. Phys. Chem. B 108 (2004) 4086.
[16] J.C. Yu, J.G. Yu, W.K. Ho, Z.T. Jiang, L.Z. Zhang, Chem. Mater. 14 (2002) 3808.
[17] J.C. Yu, W.K. Ho, J.G. Yu, S.K. Hark, K. Iu, Langmuir 19 (2003) 3889.
[18] C. Minero, G. Mariella, V. Maurino, D. Vione, E. Pelizzetti, Langmuir 16 (2000) 8964.
[19] C. Minero, G. Mariella, V. Maurino, E. Pelizzetti, Langmuir 16 (2000) 2632.
[20] C.M. Wang, T.E. Mallouk, J. Am. Chem. Soc. 112 (1990) 2016.
[21] A. Hattori, M. Yamamoto, H. Tada, S. Ito, Chem. Lett. 27 (1998) 707.
[22] H.G. Yang, H.C. Zeng, J. Phys. Chem. B 108 (2004) 3492.
[23] H.G. Yang, H.C. Zeng, J. Phys. Chem. B 108 (2004) 819.
[24] H.G. Yang, C.H. Sun, S.Z. Qiao, J. Zou, G. Liu, S.C. Smith, H.M. Cheng, G.Q. Lu, Nature 453 (2008) 638.
[25] X.G. Han, Q. Kuang, M.S. Jin, Z.X. Xie, L.S. Zheng, J. Am. Chem. Soc. 131 (2009) 3152.

[26] Y.Q. Dai, C.M. Cobley, J. Zeng, Y.M. Sun, Y.N. Xia, Nano Lett 9 (2009) 2455.
[27] F. Amano, T. Yasumoto, O.O. Prieto-Mahaney, S. Uchida, T. Shibayama, B. Ohtani, Chem. Commun. (2009) 2311.
[28] J.G. Yu, W.G. Wang, B. Cheng, B.L. Su, J. Phys. Chem. C 113 (2009) 6743.
[29] J.S. Park, W.Y. Choi, Langmuir 20 (2004) 11523.
[30] H. Kim, W. Choi, Appl. Catal. B 69 (2007) 127.
[31] K.L. Lv, Y.M. Xu, J. Phys. Chem. B 110 (2006) 6204.
[32] Y.M. Xu, K.L. Lv, Z.G. Xiong, W.H. Leng, W.P. Du, D. Liu, X.J. Xue, J. Phys. Chem. C 111 (2007) 19024.
[33] J.W. Tang, H.D. Quan, J.H. Ye, Chem. Mater. 19 (2007) 116.
[34] Q. Wang, C.C. Chen, D. Zhao, W.H. Ma, J.C. Zhao, Langmuir 24 (2008) 7338.
[35] G.S. Wu, J.P. Wang, D.F. Thomas, A.C. Chen, Langmuir 24 (2008) 3503.
[36] X.F. Cheng, W.H. Leng, D.P. Liu, Y.M. Xu, J.Q. Zhang, C.N. Cao, J. Phys. Chem. C 112 (2008) 8725.
[37] M. Pelaez, A.A. de la Cruz, E. Stathatos, P. Falaras, D.D. Dionysiou, Catal. Today 144 (2009) 19.
[38] M. Mrowetz, E. Selli, Phys. Chem. Chem. Phys. 7 (2005) 1100.
[39] M. Mrowetz, E. Selli, New J. Chem. 30 (2006) 108.
[40] K.S.W. Sing, D.H. Everett, R.A.W. Haul, L. Moscou, R.A. Pierotti, J. Rouquerol, T. Siemieniewska, Pure Appl. Chem. 57 (1985) 603.
[41] J.G. Yu, G.H. Wang, B. Cheng, M.H. Zhou, Appl. Catal. B 69 (2007) 171.
[42] J.G. Yu, S.W. Liu, M.H. Zhou, J. Phys. Chem. C 112 (2008) 2050.
[43] J.G. Yu, L.J. Zhang, B. Cheng, Y.R. Su, J. Phys. Chem. C 111 (2007) 10582.
[44] J.G. Yu, Y.R. Su, B. Cheng, Adv. Funct. Mater. 17 (2007) 1984.
[45] H.G. Yang, G. Liu, S.Z. Qiao, C.H. Sun, Y.G. Jin, S.C. Smith, J. Zou, H.M. Cheng, G.Q. Lu, J. Am. Chem. Soc. 131 (2009) 4078.
[46] J.H. Pan, X.W. Zhang, A.J. Du, D.D. Sun, J.O. Leckie, J. Am. Chem. Soc. 130 (2008) 11256.
[47] W.F. Zhang, M.S. Zhang, Z. Yin, Q. Chen, Appl. Phys. B 70 (2000) 261.
[48] M.H. Zhou, J.G. Yu, S.W. Liu, P.C. Zhai, B.B. Huang, Appl. Catal. B 89 (2009) 160.
[49] J.L. Ferry, W.H. Glaze, J. Phys. Chem. B 102 (1998) 2239.
[50] A. Selloni, Nat. Mater. 7 (2008) 613.
[51] J.G. Yu, Q.J. Xiang, J.R. Run, S. Mann, CrystEngComm 12 (2010) 872.
[52] N. Murakami, Y. Kurihara, T. Tsubota, T. Ohno, J. Phys. Chem. C 113 (2009) 3062.
[53] Y.W. Jun, M.F. Casula, J.-H. Sim, S.Y. Kim, J. Cheon, A.P. Alivisatos, J. Am. Chem. Soc. 125 (2003) 15981.
[54] B. Wu, C. Guo, N. Zheng, Z. Xie, G.D. Stucky, J. Am. Chem. Soc. 130 (2008) 17563.
[55] T. Ohno, K. Sarukawa, M. Matsumura, New J. Chem. 26 (2002) 1167.
[56] T. Taguchi, Y. Saito, K. Sarukawa, T. Ohno, M. Matsumura, New J. Chem. 27 (2003) 1304.